RESEARCH ARTICLE

A Novel Tool to Identify Bactericidal Compounds against Vulnerable Targets in Drug-Tolerant *M. tuberculosis* found in Caseum

Jansy P. Sarathy,[a] Min Xie,[a] Richard M. Jones,[b] Adrienne Chang,[c] Paulina Osiecki,[a] Danielle Weiner,[d,e] Wen-Shan Tsao,[a] Maureen Dougher,[a] Landry Blanc,[f] Nader Fotouhi,[g] Laura E. Via,[d,e] Clifton E. Barry III,[d,h] Iwijn De Vlaminck,[c] David R. Sherman,[b] Véronique A. Dartois[a,i]

[a]Center for Discovery and Innovation, Hackensack Meridian Health, Nutley, New Jersey, USA
[b]Department of Microbiology, University of Washington, Seattle, Washington, USA
[c]Nancy E. and Peter C. Meinig School of Biomedical Engineering, Cornell University, Ithaca, New York, USA
[d]Tuberculosis Research Section, Laboratory of Clinical Infectious Diseases, NIAID, NIH, Bethesda, Maryland, USA
[e]Tuberculosis Imaging Program, Division of Intramural Research, NIAID, NIH, Bethesda, Maryland, USA
[f]University of Bordeaux, CNRS, CBMN, UMR 5248, Pessac, France
[g]Global Alliance for TB Drug Development, New York, New York, USA
[h]Institute of Infectious Disease and Molecular Medicine, Faculty of Health Sciences, University of Cape Town, Cape Town, South Africa
[i]Hackensack Meridian School of Medicine, Department of Medical Sciences, Nutley, New Jersey, USA

ABSTRACT Caseous necrosis is a hallmark of tuberculosis (TB) pathology and creates a niche for drug-tolerant persisters within the host. Cavitary TB and high bacterial burden in caseum require longer treatment duration. An *in vitro* model that recapitulates the major features of *Mycobacterium tuberculosis* (Mtb) in caseum would accelerate the identification of compounds with treatment-shortening potential. We have developed a caseum surrogate model consisting of lysed and denatured foamy macrophages. Upon inoculation of Mtb from replicating cultures, the pathogen adapts to the lipid-rich matrix and gradually adopts a nonreplicating state. We determined that the lipid composition of *ex vivo* caseum and the surrogate matrix are similar. We also observed that Mtb in caseum surrogate accumulates intracellular lipophilic inclusions (ILI), a distinctive characteristic of quiescent and drug-tolerant Mtb. Expression profiling of a representative gene subset revealed common signatures between the models. Comparison of Mtb drug susceptibility in caseum and caseum surrogate revealed that both populations are similarly tolerant to a panel of TB drugs. By screening drug candidates in the surrogate model, we determined that the bedaquiline analogs TBAJ876 and TBAJ587, currently in clinical development, exhibit superior bactericidal against caseum-resident Mtb, both alone and as substitutions for bedaquiline in the bedaquiline-pretomanid-linezolid regimen approved for the treatment of multidrug-resistant TB. In summary, we have developed a physiologically relevant nonreplicating persistence model that reflects the distinct metabolic and drug-tolerant state of Mtb in caseum.

IMPORTANCE *M. tuberculosis* (Mtb) within the caseous core of necrotic granulomas and cavities is extremely drug tolerant and presents a significant hurdle to treatment success and relapse prevention. Many *in vitro* models of nonreplicating persistence have been developed to characterize the physiologic and metabolic adaptations of Mtb and identify compounds active against this treatment-recalcitrant population. However, there is little consensus on their relevance to *in vivo* infection. Using lipid-laden macrophage lysates, we have designed and validated a surrogate matrix that closely mimics caseum and in which Mtb develops a phenotype similar to that of nonreplicating bacilli *in vivo*. The assay is well suited to screen for bactericidal compounds against caseum-resident Mtb in a medium-throughput format, allowing for

Editor Steven J. Projan, MedImmune

Address correspondence to Véronique A. Dartois, veronique.dartois@hmh-cdi.org, or Jansy P. Sarathy, Jansy.sarathy@hackensackumc.org.

The authors declare no conflict of interest.

This article is a direct contribution from Véronique A. Dartois, a Fellow of the American Academy of Microbiology, who arranged for and secured reviews by Christina Stallings, Washington University in St Louis School of Medicine, and Bavesh Kana, University of the Witwatersrand.

Received 13 March 2023
Accepted 14 March 2023
Published 5 April 2023

reduced reliance on resource intensive animal models that present large necrotic lesions and cavities. Importantly, this approach will aid the identification of vulnerable targets in caseum Mtb and can accelerate the development of novel TB drugs with treatment-shortening potential.

KEYWORDS caseum, nonreplicating *Mycobacterium tuberculosis*, persister, tuberculosis, vulnerable target

In pulmonary tuberculosis (TB), the necrotic core of closed granulomas and cavities can harbor high burdens of *Mycobacterium tuberculosis* (Mtb) bacilli and is very difficult to sterilize (1–5). These necrotic foci are made of caseum, a largely acellular matrix that essentially results from necrosis of infected foamy macrophages (FM) starting from the center of the lesion (6, 7), or from a bronchiolar obstruction progressing into caseating cavitary disease (8). Preclinical and clinical studies have shown that these niches constitute reservoirs of extracellular Mtb that can persist throughout antibiotic treatment (5, 9–12) and are prone to the emergence of drug resistance (13–15). Thus, drug regimens that efficiently eradicate this bacterial subpopulation would have a positive impact on the global control of TB by improving cure rates, reducing treatment duration, and curbing the emergence of drug resistance.

In a previous study, we demonstrated that caseum-resident Mtb is profoundly tolerant to first- and second-line TB drugs by using caseum explanted from rabbit cavities (16). In this native environment, Mtb adopts a nonreplicating state and accumulates intrabacterial lipid inclusions (ILIs). ILIs are neutral lipid storage vesicles that are strongly associated with dormancy and phenotypic drug resistance in mycobacteria (17–21). Decreased susceptibility is compounded by suboptimal drug distribution in the nonvascularized caseous core of necrotic granulomas, creating pockets of subinhibitory drug concentrations and *de facto* monotherapy (22–25). The field of TB drug discovery has spent significant effort developing single and multistress nonreplicating Mtb culture models that mimic the diverse physiological states that the pathogen adopts during infection. While these models reveal that nonreplicating Mtb is tolerant to many antibiotics (18, 26–28), patterns of drug tolerance tend to be different in each assay, and a consensus is lacking as to which conditions are most predictive of preclinical and clinical efficacy (29, 30). A model that faithfully mimics the specific physiology and drug tolerance of Mtb in native caseum would be adequate to identify both active compounds and vulnerable Mtb targets in this distinctive, mostly acellular lipid-rich matrix.

Experimental findings support the notion that caseum is made primarily of necrotized FM. The foamy phenotype results from intracellular lipid accumulation in response to Mtb infection, exceeding the host cell's capacity to maintain lipid homeostasis. Host lipids are sequestered in lipid droplets (LDs), contributing to the characteristic foamy appearance. Infected FM directly surround the caseous core of TB lesions in patients and animal models (7, 31–33), becoming gradually necrotic as infection progresses, thus expanding the caseous center. Biochemical and molecular analyses revealed that FM and caseum have comparable protein and lipid compositions (7). Mtb infection of macrophages *in vitro* produces the foam cell phenotype via tumor necrosis factor receptor signaling and downstream activation of caspase pathways and the mammalian target rapamycin complex 1. In addition, reduced oxygen tension, associated with poor vascularization, and exposure to very-low-density lipoproteins and selected fatty acids trigger FM development (34–36).

Here, we attempted to deliver a predictive assay that replicates the phenotypic drug resistance of Mtb found in caseum without relying on animal infection models, starting from a caseum surrogate previously developed to estimate nonspecific drug binding in caseum (37, 38). Properties of the matrix and of the inoculated pathogens were optimized to reproduce major lipid contents of caseum, Mtb's nonreplicating status, accumulation of ILIs, regulation of specific dormancy and lipid metabolic pathways, and phenotypic resistance to major TB drugs, as seen in native caseum Mtb. To

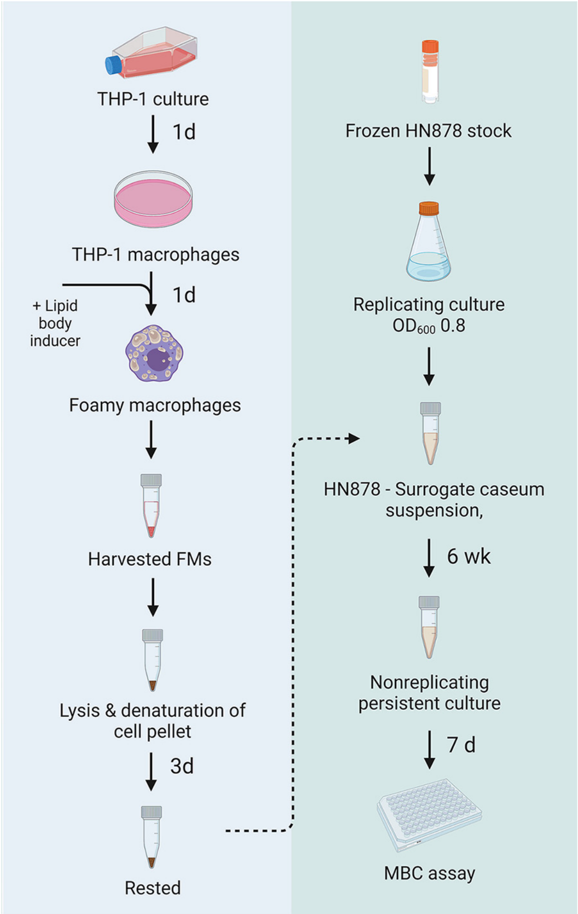

FIG 1 Illustration of the overall experimental design. THP-1 derived FM are used to generate a caseum surrogate matrix, which is spiked with *M. tuberculosis* HN878 to reproduce the typical physiologic, genetic, and phenotypic properties of caseum-resident Mtb. Image created with BioRender.

establish the utility and predictive value of the model, we characterized the bactericidal activities of novel and potent new bedaquiline analogs currently in clinical development in the *ex vivo* and surrogate caseum models. We propose that the caseum surrogate model is adequate to screen drug discovery compounds, identify vulnerable drug targets in dormant caseum Mtb, and inform the development of shorter and more effective treatment regimens.

RESULTS

To reproduce the drug-tolerant phenotype of caseum-resident Mtb (16) and develop an appropriate drug screening tool, we designed a surrogate assay consisting of THP-1-derived FM lysate inoculated with Mtb until the pathogen acquires physiological, genetic, and phenotypic properties that recapitulate those of caseum Mtb.

Reproducing the fatty acid profile, cholesterol and glyceride abundance, and pH of native caseum. To reproduce the lipid-rich environment of caseum, we first optimized lipid droplet formation and accumulation in macrophages. THP-1-derived macrophages (THPMs) were exposed to oleic acid (OA, 18:1), stearic acid (SA, 18:0), and irradiated Mtb (iMtb) for 24 h (Fig. 1), followed by staining for neutral lipid deposits and flow cytometry analysis of mean fluorescence intensities (MFI). OA-treated THPMs produced the greatest increase in lipid staining compared to nonfoamy cells (Fig. 2A; also, see Fig. S1C in the supplemental material), while both SA and iMtb treatments resulted in comparable staining. These quantitative results were confirmed visually by microscopic analyses, with the most abundant lipid droplets found within the cytosol of OA-induced macrophages (Fig. 2B). Using fluorescence microscopy, we observed

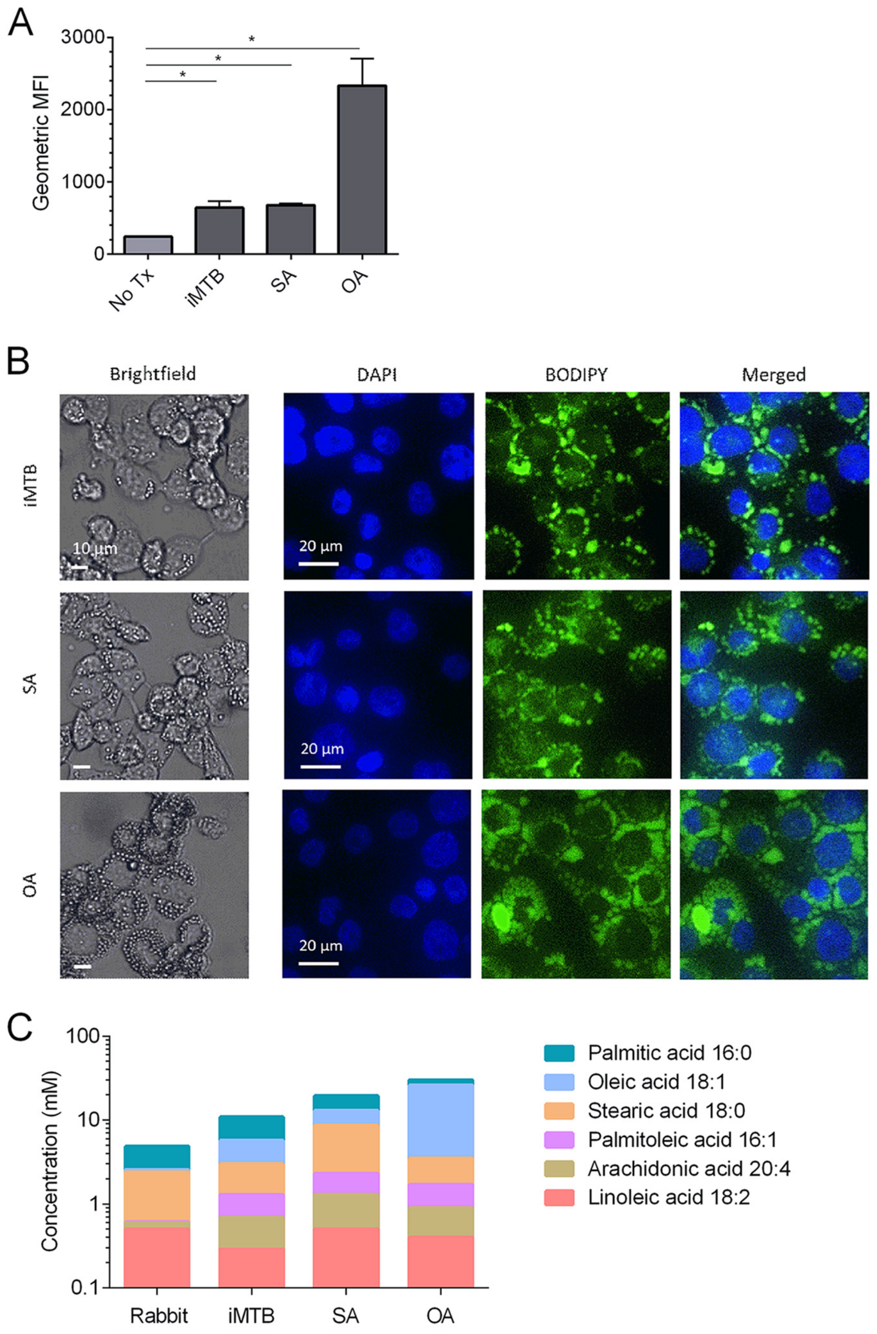

FIG 2 Quantitative and qualitative analyses of induced lipid droplets and neutral lipids in THP-1 macrophages and macrophage lysates. (A) Lipid droplet abundance in THP-1 macrophages after exposure to various foamy-cell inducers. THP-1 macrophages were treated with irradiated Mtb (iMtb; MOI, 1:50), stearic acid (SA; 100 μM), or oleic acid (OA; 100 μM) for 24 h. Lipid bodies were stained with BODIPY 493/503 prior to analysis by flow cytometry. Data are expressed as the geometric mean fluorescence intensity (MFI) for each group. Error bars represent standard deviations for three biological replicates. *, $P < 0.05$. (B) Bright-field and fluorescence microscopy images of iMtb-, SA-, and OA-induced THP-1 macrophages. Lipid droplets and nuclei were stained with BODIPY and DAPI, respectively. (C) Fatty acid quantification in rabbit caseum and surrogate caseum generated using three different inducers. The six most abundant fatty acids are shown.

that the lipophilic dye localizes to cytosolic spherical organelles surrounding the nucleus (Fig. 2B).

We then compared the glyceride, cholesterol, and fatty acid contents of the three caseum surrogates to those of native rabbit caseum. The combined concentration of

TABLE 1 Lipid and pH profile of native rabbit caseum and caseum surrogates

	Concn (mM) (mean ± SD) of:		
Caseum or surrogate	**Total glycerides[a]**	**Total cholesterol[b]**	**pH**
Rabbit caseum	3.2 ± 0.2	9.2 ± 0.1	6.5–7.1
iMtb-induced surrogate	11.2 ± 1.9	6.6 ± 0.3	6.6–6.9
SA-induced surrogate	24.8 ± 7.0	6.8 ± 0.9	6.6
OA-induced surrogate	92.9 ± 9.1	6.5 ± 0.7	6.6

[a]Inclusive of tri-, di- and monoglycerides.
[b]Inclusive of free cholesterol and cholesterol esters.

mono-, di- and triglycerides was 3.5-, 7.8-, and 29-fold higher in iMtb-, SA-, and OA-induced caseum surrogates, respectively (Table 1). The combined free cholesterol and cholesterol ester concentrations were similar in all surrogates and in native caseum (Table 1). To generate quantitative information on specific free fatty acid (FFA) species present in the various surrogates, we measured the concentrations of 23 individual species by liquid chromatography coupled to mass spectrometry (LC-MS) (Table S1). The 6 most abundant species are shown in Fig. 2C. Qualitatively, the FFA content of *ex vivo* caseum was recapitulated in the caseum surrogates, but stimulation of THPM with OA resulted in a marked enrichment of this fatty acid in the surrogate matrix (Fig. 2C and Table S1). We also showed that the pHs of iMtb-, SA-, and OA-induced surrogates (pH 6.6 to 6.9) fall within the range of pHs measured in caseum excised from rabbit cavities, lesions from C3HeB/FeJ mice and guinea pigs, and resected clinical samples (6, 39) (Table 1). Overall, the major FFA species found in rabbit caseum are best reproduced in iMtb- and SA-induced surrogate caseum.

Mtb in caseum surrogate is viable and nonreplicating. We first demonstrated that native Mtb in *ex vivo* rabbit cavity caseum exists in a nonreplicating state and maintains a stable bacterial burden for up to 4 weeks (Fig. 3A), in agreement with previous 8-day growth kinetic data (16). We then observed that replicating Mtb adopts the nonreplicating state when inoculated into *ex vivo* caseum and that bacterial burden remained stable for up to 6 weeks (Fig. 3B). To identify the caseum surrogate matrix that best supports bacterial survival and induces nonreplication of Mtb introduced exogenously, logarithmically growing Mtb was inoculated into the three caseum surrogates (Fig. 1), generating stable CFU kinetics in iMtb- and SA-induced preparations (Fig. 3C and D), which suggests that Mtb arrests replication without compromising bacterial viability. In the OA-induced surrogate, a rapid and transient reduction in recoverable bacterial burden (1 to 2 log, statistically significant) was observed within a few days postinoculation. The CFU counts were restored to starting levels by day 14 postinoculation (Fig. 3E). Given the high OA content of this matrix (~6 mg/mL) (Fig. 2D and Table S1), we tested whether this long-chain FFA may have contributed to the transient loss of culturability. We observed >90% growth inhibition at 0.5 mg/mL OA against Mtb in liquid medium (Fig. S2A). This may have contributed to the transient inability of Mtb to produce recoverable colonies on solid medium. Incubating, or "resting," the SA- and iMtb-induced surrogates at 37°C for 3 days after the denaturation step prior to Mtb inoculation greatly improved Mtb recovery in this model (Fig. S2B to D). To test the hypothesis that fresh macrophage lysates may contain microbicidal factors such as reactive oxygen and nitrogen species, we measured the lipid peroxidation product malondialdehyde as a thiobarbituric acid-reactive substance (TBARS) in each matrix. We found significantly more TBARS in SA and iMtb surrogates postrest, indicating that reactive species are dissipated via the oxidative deterioration of lipids within these matrices during the 3-day resting period (Fig. S2E).

To determine whether the apparently stable CFU kinetic profile was the result of true nonreplication or rather a balance between cell growth and death, we analyzed the pattern of metagenomic sequencing read coverage to assess genome replication (40), where nonuniform genome coverage with an overrepresentation of sequences at the origin of replication is indicative of active genome replication. Upon introduction

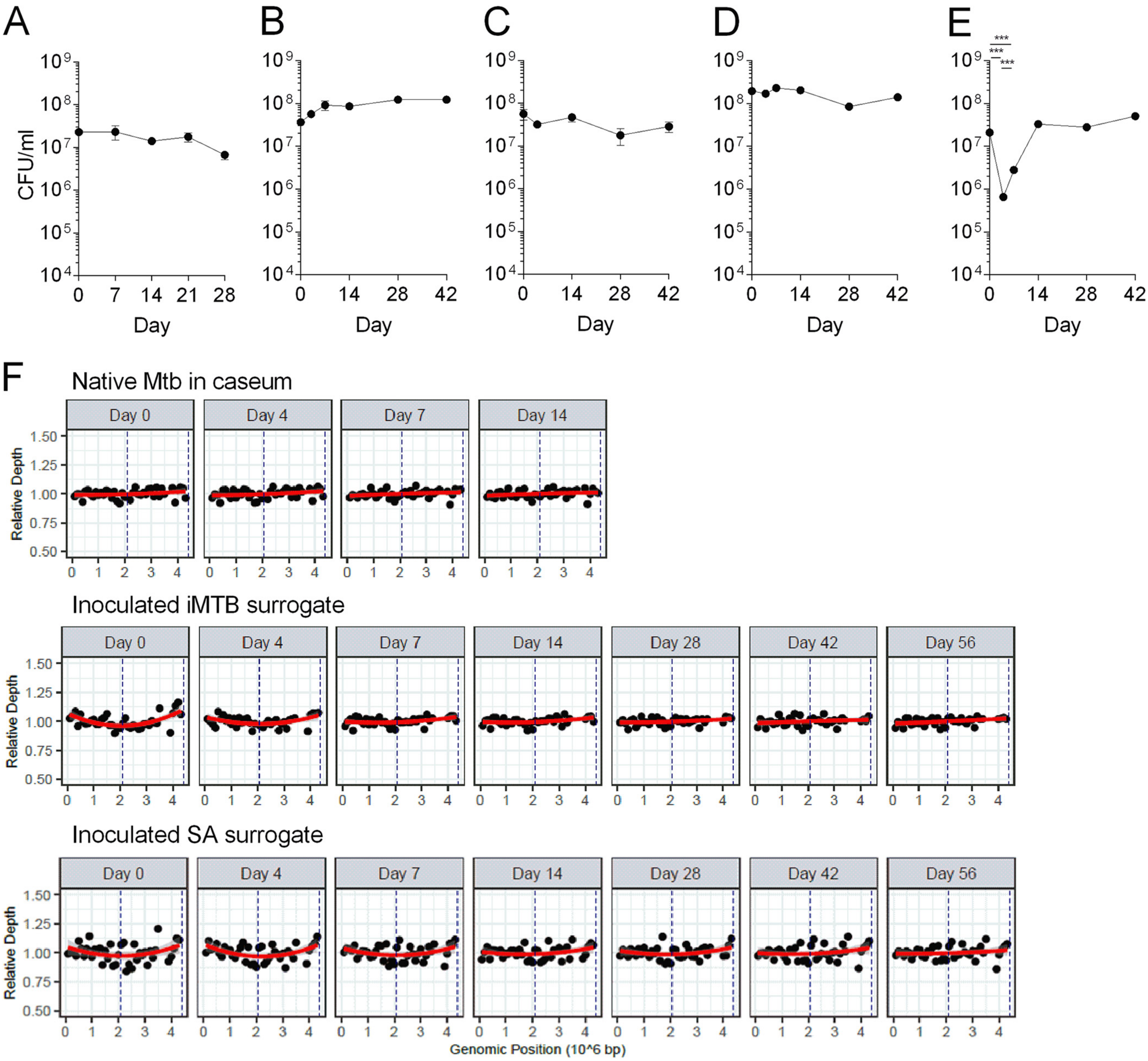

FIG 3 Growth kinetics of Mtb in caseum and surrogates. (A) Native Mtb in rabbit caseum remains in the nonreplicating state postexplantation. (B) Replicating Mtb inoculated into low-burden *ex vivo* caseum quickly adopts a viable and nonreplicating state. (C to E) Replicating Mtb was inoculated into caseum surrogates generated using (C) iMtb, (D) SA, and (E) OA as foamy-cell inducers. Error bars represent standard deviations for three technical replicates. The Mtb CFU drop observed between day 1 and day 4 or 7 in response to exposure to OA-induced caseum surrogate was statistically significant (two-tailed *t* test; ***, $P \leq 0.005$). (F) Genome sequencing coverage patterns of native Mtb in rabbit caseum and Mtb inoculated in caseum surrogates over time. Normalized genome coverage of native and inoculated Mtb are shown for a single sample in each panel. The red line is a LOESS (locally estimated scatterplot smoothing) filter smoothing curve (span = 10) with standard error shown in gray (confidence level = 0.95). The replication start and end sites are indicated by dashed blue lines at positions 4386870 and 2077870, respectively.

of Mtb from replicating cultures into native caseum or caseum surrogates, we observed increased uniformity of the microbe's genome coverage over time, indicative of gradual progression to the nonreplicating state in all matrices (Fig. 3F). Thus, both SA- and iMtb-induced caseum surrogates trigger transition to true nonreplication in Mtb.

Residence in caseum surrogate induces physiologic signatures of dormancy in Mtb. To determine whether Mtb accumulates ILIs in the surrogate caseum environment as it does in native caseum, we used dual Nile red-auramine O staining and confocal microscopy (16). In *ex vivo* caseum and in SA- or iMtb-induced surrogate caseum, a large proportion of Mtb bacilli accumulated neutral lipids and stained red (Fig. 4A). In contrast, very

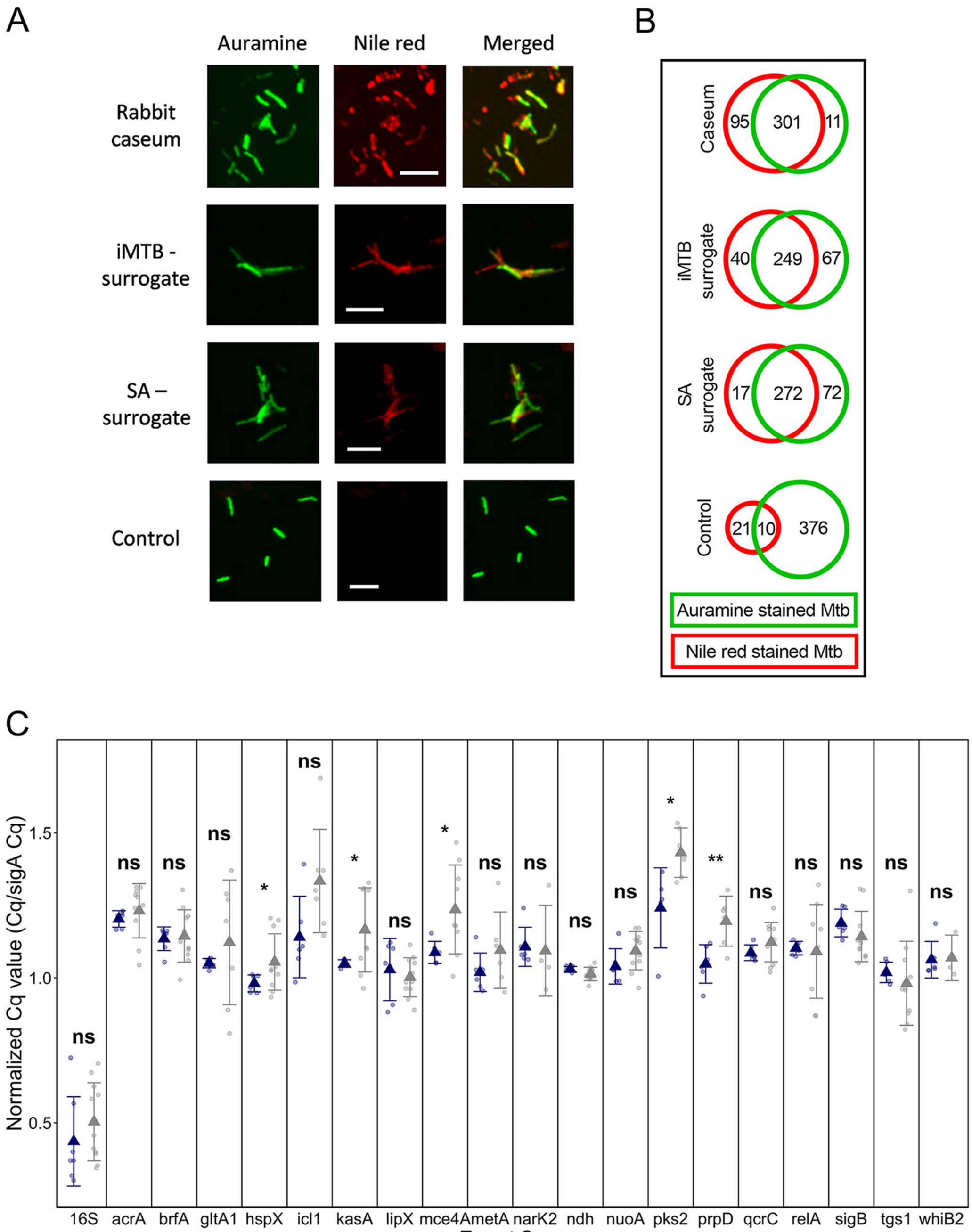

FIG 4 Intrabacterial neutral lipid accumulation in native caseum-resident Mtb, in bacilli preadapted in caseum surrogate, and in replicating (control) Mtb culture. All smears were stained with auramine O (green, acid-fast stain) and Nile red (red, neutral lipid stain) and examined by confocal laser scanning microscopy at the same laser intensity for all samples with Z-stacking to get the depth of the scan field. Bar, 5 μm. (B) Venn diagrams showing the distribution of auramine-positive and Nile red-positive bacilli in caseum, caseum surrogate, and replicating Mtb culture. (C) Plot showing Mtb gene expression across 20 loci of interest. qRT-PCR was performed on RNA extracted from Mtb-infected rabbit caseum or Mtb adapted for 6 weeks in iMtb-induced caseum surrogate. Rounded points show individual C_q values normalized to *sigA*, triangles show mean normalized C_q values, and error bars show standard deviations. Groups of normalized samples were compared using an unpaired Student's *t* test; the *P* values were adjusted using the Holm-Bonferroni method. ns, not significant ($P > 0.05$); *, $P \leq 0.05$; **, $P \leq 0.01$.

few bacilli appeared Nile red positive in replicating Mtb cultures. Magnification of individual Nile red-positive bacilli revealed the formation of distinct ILIs. Quantification of Nile red- and auramine O-stained bacilli confirmed a dramatic increase in neutral lipid accumulation in caseum and the surrogates compared to replicating Mtb cultures (Fig. 4B). In

TABLE 2 Nonreplicating Mtb gene expression in freshly excised rabbit caseum and iMtb-induced caseum surrogate

		Mean normalized expression value in:	
Category and gene identifier	**Gene name**	**Caseum**	**Caseum surrogate**
Cell wall biosynthesis			
Rv3825c	*pks2*	1.43	1.24
Rv2245	*kasA*	1.16	1.04
Lipid metabolism			
Rv1169c	*lipX*	1.00	1.03
Rv3130c	*tgs1*	0.98	1.02
Respiration			
Rv0467	*icl1*	1.33	1.14
Rv2194	*qcrC*	1.12	1.09
Rv1854c	*ndh*	1.01	1.03
Rv3145	*nuoA*	1.09	1.04
Rv2583c	*relA*	1.09	1.10
Rv1131	*gltA1/prpC*	1.12	1.05
Rv3341	*metA*	1.10	1.02
Rv1130	*prpD*	1.20	1.05
Transcription			
Rv2710	*sigB*	1.14	1.19
Rv3260c	*whiB2*	1.07	1.06
Virulence, detoxification, adaptation			
Rv2031c	*hspX*	1.05	0.98
Rv3499c	*mce4A*	1.24	1.09
Transporters			
Rv1737c	*narK2*	1.09	1.11
Iron storage			
Rv1876	*bfrA*	1.14	1.13

summary, neutral lipid accumulation is a defining feature of nonreplicating Mtb in caseum and caseum surrogates. Next, we compared the expression of 20 genes (18 selected genes, plus *sigA* and 16S rRNA as references) with diverse functions in native caseum Mtb and Mtb preadapted in caseum surrogate (Table 2). These genes are involved in cell wall biosynthesis, lipid metabolism, respiration, virulence and detoxification, transmembrane transport, and iron storage and were selected for their putative roles in nonreplicating persistence models. Relative gene expression in caseum surrogate was quantified by quantitative reverse transcription-PCR (qRT-PCR), normalized to *sigA* expression, and calibrated against expression levels in *ex vivo* caseum. Relative gene expression between caseum and the surrogate was not significantly different (Student's *t* test; $P > 0.05$) for 15 of the 18 genes studied (Fig. 4C). Additionally, when average normalized quantification cycle (C_q) values between caseum and surrogate samples were compared for 19 genes (16S excluded), there was a significant correlation (Pearson's correlation; $R = 0.74$; $P < 0.005$) (Fig. S3). Altogether, these data indicate that the surrogate model recapitulates selected features of the physiologic and metabolic state of Mtb in *ex vivo* caseum.

Mtb gradually develops phenotypic resistance to major TB drugs in caseum surrogate. Exponentially growing Mtb was inoculated into caseum surrogate and preadapted for 4, 6, and 8 weeks prior to incubation with a panel of TB drugs (Fig. 1). The assay was designed to generate the 90% minimal bactericidal concentration in caseum (casMBC$_{90}$) or in surrogate (srgMBC$_{90}$) to infer potency and Δlog CFU$_{max}$ or maximum killing effect (E_{max}) to infer sterilizing potential at the highest concentration (Table 3). Isoniazid and delamanid were excluded from the study because of significant instability in both matrices (Fig. S4A). We found that drug tolerance in caseum was best reproduced

TABLE 3 Bactericidal activity of TB drugs against replicating Mtb cultures, native bacteria in caseum, and Mtb preadapted in iMtb-induced surrogate caseum for 6 weeks

		Caseum		Caseum surrogate	
Drug	Replicating Mtb MBC_{90} (μM)[a]	MBC_{90} (μM)	ΔLog CFU_{max}	MBC_{90} (μM)	ΔLog CFU_{max}
Pyrazinamide	>80	>512	0.5	>512	0.1
Ethambutol	2.5–5	>512	0.2	90	1.1
Rifampicin	0.07	10	3.5	2.5	4.6
Rifapentine	0.08	10	3.1	2.2	4.4
Rifabutin	0.04	1	4.0	1.5	4.3
Moxifloxacin	0.3–0.6	1.6	1.8	1.5	1.8
Levofloxacin	0.3–2.5	9	1.8	9	1.3
Gatifloxacin	0.6	1.5	1.9	3.5	1.4
Linezolid	10	>512	0.2	>512	0.5
Sutezolid	1.4–5.7	16	1.4	8	1.6
Pretomanid	0.6	70	1.6	63	2.0
SQ109	0.8–2.3	260	1.8	200	1.8
Bedaquiline[b]	3.6–10	4.7	1.9	5.4	1.6
Kanamycin	5	>512	0.0	512	1.0
Clofazimine	40	>128	0.7	>128	0.1

[a]MBC_{90}s in replicating bacteria were measured after 5 days of incubation (66, 80).
[b]Bedaquiline was tested in 14-day assays in caseum and surrogate instead of the standard 7-day incubation period.

after 6 weeks of Mtb preadaptation in surrogate, as measured by MBC_{90} (Table S2). After 6 weeks, the $srgMBC_{90}$/$casMBC_{90}$ ratio for all drugs tested clustered most closely around 1 (Fig. S4B). Given bedaquiline's slow onset of action (41, 42), its bactericidal activity was evaluated after 7 (standard) and 14 days of incubation. Bedaquiline's $casMBC_{90}$ was 14-fold lower in the 14-day assay than in the 7-day assay (Fig. S4C). A robust correlation between $srgMBC_{90}$ and $casMBC_{90}$ was obtained (R^2 = 0.78) (Fig. 5A). Similarly, we obtained a good correlation between Δlog CFU_{max} in the *ex vivo* and *in vitro* assays (R^2 = 0.82) (Fig. 5B), indicating comparable phenotypic drug resistance in both matrices. Rifamycins were among the most potent drugs in caseum and exhibited the highest sterilizing activity (Fig. 5B). We also compared the magnitude of the drug tolerance induced by caseum versus the widely used nutrient and oxygen starvation conditions (Fig. 5C) (26, 27, 43, 44). The intracaseum potencies of rifampicin, rifapentine, kanamycin, and clofazimine are best reproduced during nutrient starvation, while bedaquiline's is recapitulated under hypoxia. The fluoroquinolones display a distinct potency profile, performing better in caseum and caseum surrogate (MBC_{90}s $\leq$ 10 μM) than in the other nonreplicating (NRP) models, with the exception of moxifloxacin being equally active under hypoxic conditions. The $casMBC_{90}$s and $srgMBC_{90}$s of rifampicin and moxifloxacin are achieved in caseum in patients receiving clinically approved doses, whereas linezolid and clofazimine are inactive within their respective intracaseum exposure windows (Fig. S5) (25).

Screening of development compounds identifies TBAJ876 and TBAJ587 as potent drug candidates in caseum. To validate the surrogate assay as a new screening platform, we measured the MBCs of a series of discovery compounds in caseum surrogate and identified the bedaquiline analogs TBAJ876 ($srgMBC_{90}$ = 0.3 μM) and TBAJ587 ($srgMBC_{90}$ = 3.2 μM) as potent agents against nonreplicating Mtb persisters in 7-day assays (Fig. 6A). We then repeated the measurements in *ex vivo* caseum and found similar MBC_{90}s and comparable E_{max} values (Fig. 6B). We replaced bedaquiline with either TBAJ876 or TBAJ587 in the bedaquiline-pretomanid-linezolid (BPaL) regimen, which was highly successful against drug-resistant TB in the pivotal Nix-TB trial (45). To directly compare the contribution of the TBAJ analogs and bedaquiline to the killing of caseum Mtb in the Nix-TB background, the concentrations of pretomanid (Pa) and linezolid (L) were fixed at their estimated average concentrations achieved in caseum over the 24-h dosing interval (C_{ave}[0–24]), and the concentration of bedaquiline, the TBAJ compounds, and their active metabolites were increased in 4-fold increments, centered on the C_{ave}[0–24]. We measured a combined 1-log killing at TBAJ concentrations that were approximately 16-fold lower than

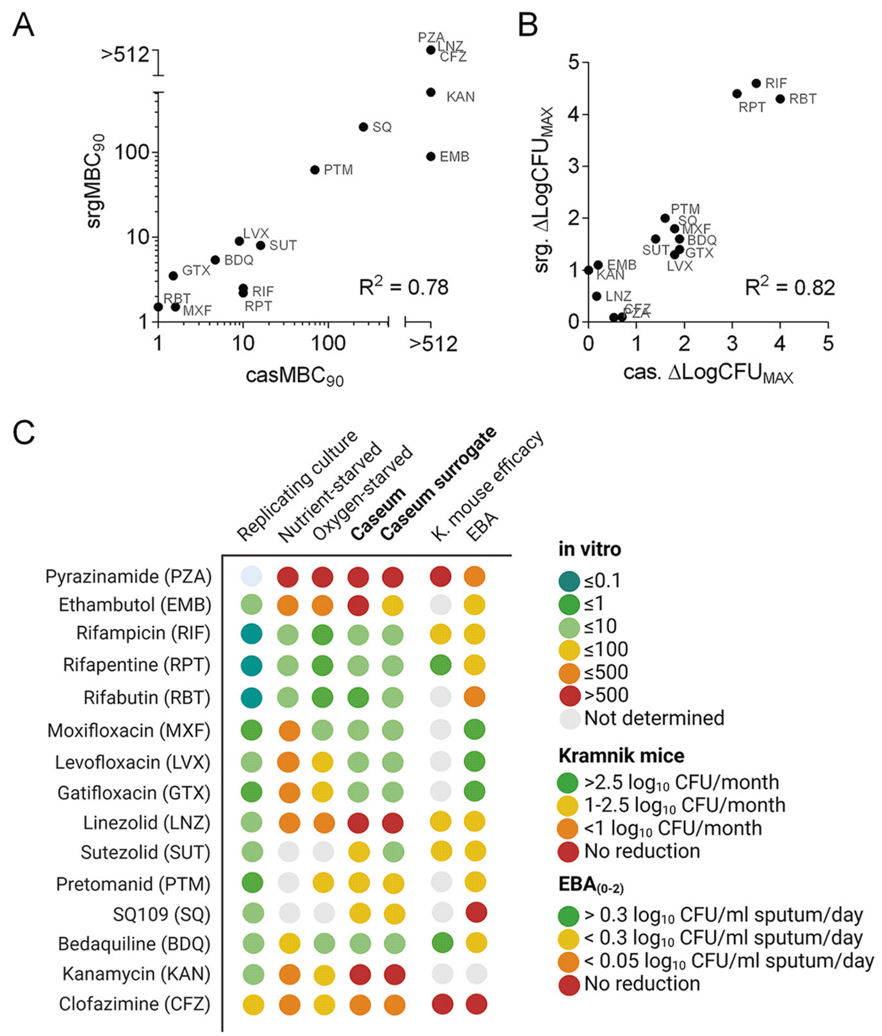

FIG 5 Comparative bactericidal activity of TB drugs against Mtb in caseum and in iMtb-induced caseum surrogate. (A) Correlation between bactericidal activity in caseum ($casMBC_{90}$) and surrogate caseum ($srgMBC_{90}$). Drug abbreviations are provided in panel C. (B) Correlation between maximal CFU reduction at the highest assay concentration ($\Delta\log CFU_{512\mu M}$) in caseum (cas) and surrogate caseum (srg). (C) Heat map of potencies of first- and second-line drugs and compounds in clinical development against Mtb in replicating cultures, in two *in vitro* models of nonreplicating persistence (66), and in native and surrogate caseum. Efficacies in the C3HeB/FeJ mouse model of necrotic lesions (12, 24, 67–69) and in phase IIa early bactericidal activity (EBA) trials (70–79) are shown as *in vivo* references. Image created with BioRender.

that of bedaquiline. The E_{max} of the TBAJ-based combinations was greater than that of Nix-TB at TBAJ concentrations 4-fold lower than that of bedaquiline (Fig. 6C). These results show that the improved potency of TBAJ analogs against replicating Mtb (46, 47) translates into increased bactericidal activity against caseum persisters compared to bedaquiline and may guide dose selection in future clinical trials. Thus, the surrogate model enables screening for compounds that are active against drug-tolerant caseum Mtb and may have treatment-shortening potential.

DISCUSSION

Phenotypic screens that mimic host-relevant environmental conditions to accurately reflect the multiple physiological states of Mtb during infection are invaluable tools for understanding Mtb's dormancy adaptations and discovering drugs that kill these populations. Animal models of TB infection reveal that caseous necrosis is associated with high bacterial burdens and limited drug-mediated sterilization (39, 48, 49). Positron emission

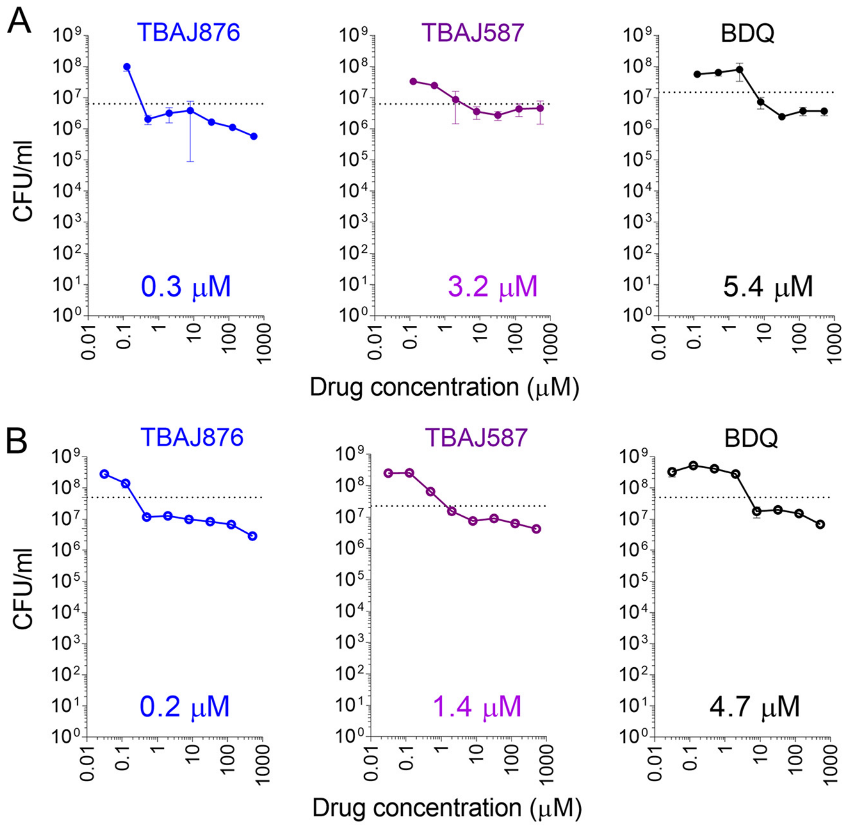

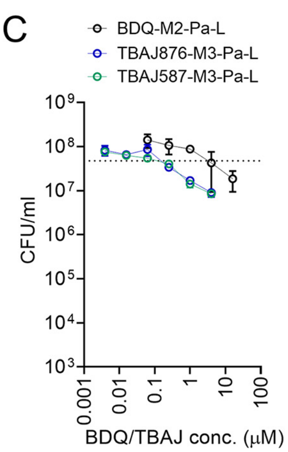

Regimen	Concentration ranges (μM)					
BDQ	0.0156	0.0625	0.25	1	4	16
BDQ-M2	0.0312	0.125	0.5	2	8	32
Pa	8	8	8	8	8	8
L	15	15	15	15	15	15
T876	0.0039	0.0156	0.0625	0.25	1	4
T876-M3	0.0078	0.0312	0.125	0.5	2	8
Pa	8	8	8	8	8	8
L	15	15	15	15	15	15
T587	0.0039	0.0156	0.0625	0.25	1	4
T587-M3	0.0078	0.0312	0.125	0.5	2	8
Pa	8	8	8	8	8	8
L	15	15	15	15	15	15

FIG 6 Bactericidal activity of bedaquiline (BDQ) analogs against Mtb persisters. TBAJ876 (blue), TBAJ587 (purple), and bedaquiline (black) were tested in (A) caseum surrogate and (B) rabbit caseum MBC assays for 14 days. The MBC_{90} of each compound is shown. (C) Bactericidal activity of bedaquiline and the TBAJ analogs in combination with pretomanid (Pa) and linezolid (L) in rabbit caseum. The des-methyl active metabolites of BDQ (M2) and TBAJ compounds (M3) are included at concentrations that reproduce their proportion relative to the parent drug in caseum. Concentration ranges used for each drug are shown in the table (T876, TBAJ876; T587, TBAJ587). The dotted line indicates a 1-log reduction in bacterial burden compared to day 1. Data points and error bars represent the means and standard deviations for three technical replicates each.

tomography-computed tomography (PET-CT) scans from TB patients illustrate the bronchial spread of infection from caseous cavities through the lungs and show that cavitary lesion dynamics is a major determinant of treatment outcome (5). Hence, predictive screening platforms that model the profound drug tolerance of caseum-resident Mtb are needed to identify promising therapeutic options. We have successfully optimized a caseum model which reproduces the extreme phenotypic drug resistance levels of caseum-resident Mtb for a range of TB drugs with diverse targets, and in which the starting inoculum is fully controlled.

In contrast, caseum specimens excised from rabbits typically contain 10^5 to 10^9 Mtb bacilli per g but include occasional very-low-burden cavities (16, 39).

Given the critical link between Mtb adaptations to lipid-rich environments, intrabacterial lipid accumulation, nonreplicating persistence, and drug tolerance (19, 31, 50), we focused on producing a surrogate with a caseum-like lipid profile by using biochemical and biological triggers known to induce lipid body accumulation in macrophages. Based on triacylglycerol (TAG), FFA, and cholesterol quantitation, we determined that while OA most effectively stimulates lipid body accumulation, the OA-induced surrogate least resembled the biochemical composition of *ex vivo* rabbit caseum due to overrepresentation of TAG and OA. It is also inherently bactericidal to Mtb at high concentrations, like other long-chain FFAs (51, 52), causing a dip in CFU upon Mtb inoculation. SA, on the other hand, is one of the most abundant FFAs in FM and caseum (7, 19), does not affect the growth or survival of Mtb, and is internalized and incorporated unchanged into phthiocerol dimycocerosate (PDIM) (53). SA- and iMtb-induced surrogate matrices adequately reproduce the host lipid profile of *ex vivo* caseum and halt Mtb replication while preserving viability, key features of nonreplicating culture models of Mtb dormancy. Both iMtb and SA can be used as lipid droplet inducers, providing the option to avoid confounding bacterial proteins, genetic material, or lipids present in iMtb, which could interfere with -omics analyses.

In mycobacteria, intrabacterial TAG accumulation is associated with low metabolic activity, growth arrest, loss of acid fastness, and phenotypic drug resistance (54). These ILI TAG stores serve as long-term energy sources during periods of stress and enable mycobacterial persistence (55). Accordingly, we observed ILI accumulation in Mtb in the *ex vivo* and surrogate models and corresponding expression of lipid metabolism genes. The gradual increase in Mtb drug tolerance up to 8 weeks postinoculation in caseum surrogate is the result of continuous adaptations of the pathogen in response to changes in its environment. The transition to a lipid-rich diet triggers rapid metabolic and physiologic adaptations, such as accumulation of ILIs. We hypothesize that this is followed by a slower process of matrix/pathogen coevolution, whereby gradual nutrient and oxygen depletion (the plates are sealed and incubated without agitation) as well as spontaneous hydrolysis of glycerides, oxidation of fatty acids and other lipids, and the decay of macromolecules collectively trigger a slow but profound dormancy program inducing phenotypic drug resistance. Drug tolerance reaches a “Goldilocks” state around 6 weeks postinoculation and exceeds caseum-induced drug tolerance for a subset of drugs after 8 weeks of preincubation in the surrogate (Fig. S4B). Our model provides a unique tool to investigate the matrix/pathogen coevolution using biochemical and transcriptome sequencing (RNA-Seq) methods and identify the determinants of the excessive drug tolerance observed at 8 weeks.

Overall, the caseum surrogate model better recapitulates the drug tolerance profile of Mtb in *ex vivo* caseum than other commonly employed NRP models and provides one answer to the long-standing question of identifying a clinically relevant assay of nonreplicating persistence (56). Rifamycins and fluoroquinolones are most potent, and the caseum model accurately ranks potencies within drug classes (rifabutin $>$ rifapentine $\approx$ rifampicin; moxifloxacin $>$ gatifloxacin $>$ levofloxacin, as observed in native caseum), making it an excellent screening tool for lead optimization in TB drug discovery. As measured by Δlog CFU$_{max}$ or E_{max}, rifamycins are the most effective sterilizers in native and surrogate caseum, highlighting the potential of novel RpoB inhibitors against dormant Mtb. The robust correlation between Δlog CFU$_{max}$ in caseum and the surrogate further validates the model, which was recently exploited to confirm CinA as a major determinant of drug tolerance in Mtb (57). Comparing the bactericidal activity of the study drugs in native and model caseum to clinical concentrations achieved in the cavity caseum of TB patients, measured for a subset of 6 drugs (15, 25), revealed that rifampicin and moxifloxacin achieve bactericidal concentrations in caseum, consistent with recent promising results of the first ever 4-month regimen containing rifapentine and moxifloxacin in the treatment of drug-susceptible TB (58). TBAJ876 and

TBAJ587 were identified as potent bactericidal drug candidates in the caseum surrogate model and improved the bactericidal activity of the recently approved bedaquiline-pretomanid-linezolid regimen for multidrug-resistant TB against caseum Mtb (45). Upcoming clinical trials will confirm whether this promising result translates into shortening of treatment for multidrug-resistant TB.

Potential limitations of this study are the use of rabbit caseum to calibrate the model, which may not fully recapitulate the properties and drug tolerance of clinical caseum Mtb, and the use of THP-1 cells, which, while easy to handle and robust, are not completely representative of primary macrophages from which foamy macrophages emerge in human lesions. On the other hand, the choice of THP-1 cells will facilitate implementation of the assay by other investigators, the lab-to-lab reproducibility of which will be the focus of follow-up studies.

The assay is amenable to medium-throughput screening to identify compounds active against nonreplicating persistent Mtb in cavity caseum, is cost-effective, and circumvents the need to infect animals. In addition to measuring bactericidal activity, the tool can be adapted to identify vulnerable bacterial targets and study chemical genetic interactions in caseum Mtb, using high-density insertional mutagenesis or CRISPRi genetic knockdown libraries (59, 60). In combination with DiaMOND, an emerging platform to predict high-order drug interactions (61) and *in vivo* treatment outcomes (30), the model can also be leveraged to identify translatable synergistic drug combinations that sterilize cavity caseum and may shorten TB chemotherapy duration.

MATERIALS AND METHODS

Chemicals and cell lines. Moxifloxacin and linezolid were purchased from Sequoia Research Products (Berkshire, UK) while rifapentine, rifabutin, pyrazinamide, sutezolid, and clofazimine were purchased from Sigma-Aldrich (St. Louis, MO). Rifampicin and levofloxacin were purchased from Gold Biotechnology (St. Louis, MO) and ChemImpex Intl Inc. (Wood Dale, IL), respectively. Kanamycin sulfate, gatifloxacin, and ethambutol dihydrochloride were purchased from Fisher Scientific (Hampton, NH). Pretomanid was obtained from BioDuro (San Diego, CA). Bedaquiline was provided by Janssen Research and Development (Raritan, NJ). TBAJ876 and TBAJ587 were provided by the TB Alliance (Pretoria, South Africa). SQ109 was provided by Sequella, Inc. (Rockville, MD). Oleic acid (OA) and stearic acid (SA) were obtained from MP Biomedicals (Irvine, CA) and Alfa Aesar (Haverhill, MA), respectively. *Mycobacterium tuberculosis* HN878 and gamma-irradiated whole HN878 cells were obtained from BEI Resources (Manassas, VA). The human monocytic leukemia cell line THP-1 was obtained from the American Type Culture Collection (ATCC) (Manassas, VA).

Rabbit infection model and caseum collection. New Zealand White (NZW) rabbits were used for aerosol infection by *M. tuberculosis* HN878, as previously described (62). Briefly, rabbits were exposed to Mtb-containing aerosol using a nose-only delivery system. The infection was allowed to progress for 12 to 40 weeks prior to necropsy and the collection of caseum from both closed and cavitary lesions. Animal studies were carried out with approval from the Institutional Animal Care and Use Committees of the National Institute of Allergy and Infection Disease, NIH, MD (protocol number LCIM-3), or Hackensack Meridian Health, NJ (protocol number 270).

Generation of foamy macrophages and surrogate caseum. The THP-1 monocytic cell line was cultured in RPMI 1640 supplemented with 10% fetal bovine serum (FBS) and 2 mM L-glutamine. Cells were seeded on 150-mm dishes (1×10^6 cells/mL) and differentiated with 100 nM phorbol 12-myristate 13-acetate (PMA). Intracellular lipid accumulation was stimulated overnight using OA, SA, or iMtb. OA was added at 0.4 mM as described previously (37). SA was dissolved in ethanol and added to the culture at 0.1 mM. iMtb was used to treat THP-1 macrophages at a multiplicity of infection (MOI) of 1:50. Incubation concentrations of OA and SA above 400 μM and 100 μM, respectively, and treatment with iMtb at MOI greater than 1:50 compromised monolayer adherence and subsequent surrogate caseum recovery. After 24 h, lipid body production was confirmed using a light microscope, and foamy macrophages were detached with 5 mM EDTA, washed three times with PBS, and pelleted by centrifugation. These pellets were subjected to three freeze-thaw cycles to achieve cell lysis, followed by a 30-min incubation period at 75°C to achieve protein denaturation. Caseum surrogate was rested at 37°C for 3 days and stored at −20°C.

Flow cytometry. THPMs were cultured in 12-well plates at 1×10^6 cells per well and treated with OA, SA, or iMtb as described above. The cells were fixed with 4% paraformaldehyde, treated with 5 μM BODIPY 493/503 for 30 min and rinsed with 0.5% bovine serum albumin (BSA) in PBS. Samples were analyzed on a BD LSR Fortessa flow cytometer. BODIPY staining was assessed in the fluorescein isothiocyanate (FITC) channel. A total of 35,000 events were measured from each sample and gated as described in Fig. S1A and B.

Fluorescence microscopy. THP-1 cells were cultured on Lab-Tek chamber slides with 8 chambers each and treated as described above. The slides were washed with PBS, fixed in 4% paraformaldehyde for 30 min, and stained with 10 μM BODIPY 493/503 (Invitrogen, Waltham, MA) in PBS in the dark for 20 min. After three washes, cells were stained with 300 nM 4′,6-diamidino-2-phenylindole (DAPI) in PBS for 5 min.

After 3 final PBS washes, slides were mounted with ProLong Gold antifade reagent (Invitrogen) and left to cure overnight at room temperature. The stained cells were observed with a Nikon Eclipse Ti fluorescence microscope under a 40× objective.

TBARS assay. Malondialdehyde contents in each surrogate caseum preparation were measured using the TBARS assay kit (R&D Systems). Caseum surrogates were homogenized in water (1:9 [wt/vol]), precipitated with equal volumes of acid reagent, and incubated with TBA reagent as instructed by the manufacturer.

Genomic DNA sequencing to assess bacterial growth dynamics. Total DNA was extracted from rabbit caseum homogenates containing native Mtb or caseum surrogate homogenates containing preadapted Mtb using the QIAamp Fast DNA tissue kit (Qiagen, Germantown, MD) and heat inactivation at 90°C for 30 min. Sequencing libraries were prepared using the Nextera XT DNA library preparation kit (Illumina, San Diego, CA). Samples were pooled and sequenced on the Illumina NextSeq platform (paired end, 2 × 75 bp). Low-quality bases and Illumina-specific reads were trimmed (Trimmomatic-0.32, LEADING:3 TRAILING:3 SLIDINGWINDOW:4:15 MINLEN:30) (63). Reads were merged using FLASH-1.2.7 and aligned (BWA-mem) against the rabbit genome (GCF_000003625.3) (64). Unaligned reads were extracted and aligned to the circularized *Mycobacterium tuberculosis* H37Rv genome (edited from NC_000962.3). Bacterial genome replication dynamics were visualized using the approach described by Burnham et al. (65).

Host lipid quantitation. Total glyceride and cholesterol quantification were achieved using colorimetric kits (BioVision, Inc., Milpitas, CA) as instructed by the manufacturer. For TAG quantification, caseum and surrogate samples were homogenized in a 5% NP-40 solution (1:9 [wt/vol] dilution), heated to 90°C and cooled to completely solubilize all TAG. For total cholesterol quantification, samples were homogenized in chloroform–isopropanol–NP-40 (7:11:0.1). Dissolved lipids were dried down completely and dissolved in the assay buffer.

Specific FFA species in all matrices were quantified by LC-MS. Twenty-five microliters of 3×-diluted homogenates were extracted with 225 μL of acetonitrile, and insoluble material was removed by centrifugation. Palmitic acid-D_{31} (Avanti Polar Lipids) was included in the analysis as an internal standard. Calibration standards for quantification were prepared in the range of 1 to 50,000 ng/mL for each FFA listed in Table S1 (Avanti Polar Lipids). LC-MS analysis was performed on a Q Exactive high-resolution mass spectrometer (Thermo Fisher Scientific, MA) coupled to a Thermo Scientific Dionex UltiMate 3000 binary system. Chromatography was performed with a Kinetex C_{18} column (2.1 by 50 mm; particle size, 1.7 μm; Phenomenex, Torrance, CA) using reverse-phase gradient elution. FFA species were quantified as $[M-H]^-$ adducts and identified based on retention time and exact mass referenced to the Lipid Maps database.

pH determination for caseum and surrogates. pH measurements were made as described previously (39). A thin layer of each caseum surrogate was applied on prewetted pH 5.1 to 7.2 pH indicator strips (VWR Chemicals BDH).

Nile red staining and confocal microscopy. Fixed smears were stained with auramine O (Remel, Lenexa, KS, USA) for 15 min, rinsed, decolorized with 3% acid alcohol (Remel) for 3 min, rinsed again, stained with 10 μg/mL Nile red in ethanol for 15 min, and rinsed again. After a 1-min incubation with potassium permanganate and a final rinse, smears were mounted with ProLong Gold antifade reagent. Images were acquired by confocal laser microscopy at 561 nm (excitation) and 582 to 622 nm (emission) for the red channel and 489 nm (excitation) and 522 to 542 nm (emission) for the green channel, using an A1 confocal microscope (Nikon, Tokyo, Japan). Three-dimensional reconstruction and deconvolution of areas of interest were performed on 19 to 25 sections. Images were analyzed using NIS Elements software (Nikon). For quantitative comparison, we counted the number of Nile red- and auramine-stained Mtb in >350 individual bacilli from multiple microscopic scans of each experimental arm.

Gene expression profiling. Specific gene expression in native Mtb in rabbit caseum and in preadapted bacteria in caseum surrogate was compared by qRT-PCR. Approximately 100 mg of fresh rabbit caseum specimens from a 12- to 40-week Mtb-infected rabbit or 100 mg of caseum surrogate with an approximate bacterial burden of 10^8 CFU/g was used in each RNA isolation preparation. Caseum specimens were processed immediately upon excision from pulmonary granulomas and cavities. Mtb genomic DNA (gDNA) was used as a positive control for amplification. All samples were resuspended in 1 mL of TRIzol (Invitrogen). The suspensions were initially disrupted at maximum speed on a Fisherbrand Bead Mill 24 homogenizer along with 0.1-mm zirconia/silicon beads (BioSpec Products), followed by further disruption of the Mtb using Lysing Matrix B tubes (MP Biomedicals). Total RNA was extracted using phenol-chloroform in a heavy-phase Lock Gel I tube (QuantaBio) followed by column purification using the Qiagen RNeasy kit (Qiagen). An on-column DNase digest was performed using DNase I (Qiagen) in RDD buffer. RDD buffer is a component of the RNase-Free DNase Set. After column purification, an additional DNase digest was performed using Ambion Turbo DNase treatment. Reverse transcription was carried out using SuperScript III reverse transcriptase (Invitrogen). Matched samples were included without the addition of reverse transcriptase as controls. Quantitative PCR was performed on a Bio-Rad CFX384 real-time PCR detection system using iTaq Universal SYBR green Supermix (Bio-Rad). Each plate used included the reference gene (*sigA*) to account for any variability across days or plates. Primers are listed in Table S3. Reverse PCR amplification conditions consisted of 30 s at 95°C, followed by 40 cycles of 5 s at 95°C and 30 s at 60°C, followed by melting curve analysis from 65 to 95°C with 0.5°C increments at 5 s/step. Data were analyzed using R version 4.1.2 using the tidyverse, ggpubr, and ggrepel packages. The *sigA* locus was used as the endogenous control for normalization; for each target gene, the C_q values were divided by those from the matched *sigA* control to generate normalized C_q values. Groups of normalized C_q values from either mimic or rabbit samples were compared using an unpaired Student's *t* test, and the *P* values were adjusted using the Holm-Bonferroni method.

MBC assays. The minimum bactericidal concentration assay against *M. tuberculosis* found in rabbit caseum was performed as described previously (37). casMBC$_{90}$ is defined as the minimum concentration that killed 90% of bacteria residing in caseum. The bactericidal assay was adapted for use with caseum surrogate. HN878 was grown in 7H9 Middlebrook medium supplemented with 10% albumin dextrose catalase supplement (ADC), 0.2% glycerol, and 0.05% Tween 80 to an optical density at 600 nm (OD$_{600}$) of 0.6 to 0.9. The culture was centrifuged and resuspended in water to an OD of 0.8. This cell suspension was added to the surrogate caseum pellets in a ratio of 2:1 (vol/wt). Suspensions were briefly homogenized with 1.4-mm zirconia beads. Mtb adapted to the surrogate matrix for 6 weeks at 37°C, unless specified otherwise. Subsequently, the mixture was exposed to test compounds in the range of 0.031 μM to 512 μM for 7 days, unless specified otherwise. srgMBC$_{90}$ is defined as the minimum concentration that killed 90% of bacteria residing in the caseum surrogate. ΔLog CFU$_{max}$ is defined as the logarithmic function of the net decrease in bacterial burden between the untreated (vehicle-only) condition and the highest drug concentration tested. The drug combination bedaquiline-pretomanid-linezolid was designed by centering the concentration range on the casMBC$_{90}$ of individual drugs with 4-fold increments between data points (Fig. 6C, right).

SUPPLEMENTAL MATERIAL

Supplemental material is available online only.
FIG S1, PDF file, 0.1 MB.
FIG S2, TIF file, 0.7 MB.
FIG S3, TIF file, 0.3 MB.
FIG S4, TIF file, 0.4 MB.
FIG S5, TIF file, 1.1 MB.
TABLE S1, PDF file, 0.1 MB.
TABLE S2, PDF file, 0.1 MB.
TABLE S3, PDF file, 0.1 MB.

ACKNOWLEDGMENTS

This work was conducted with support from the Bill and Melinda Gates Foundation (V.A.D., grant INV-004704; C.E.B., INV-1162695) and by the NIAID Intramural Research Program (C.E.B. and L.E.V.).

We are grateful to Jackie Ernest and Radojka Savic, of UCSF, for recommending clinically relevant drug concentration ranges in the caseum MBC combination assays. We thank ChenYu Tsai for his assistance in flow cytometry experiments and the TBIP members for assistance with the rabbit model at NIH. We thank Martin Gengenbacher and Thomas Dick for scientific discussions. We thank the TB Alliance and Sequella Inc. for providing TBAJ876, TBAJ587, and SQ109.

We have no competing interests to declare.

J.P.S., V.A.D., and N.F. designed and guided the study; J.P.S., P.O., and M.D. performed all cell culture work; J.P.S. optimized and validated the surrogate caseum; J.P.S. and M.X. determined drug efficacy; R.M.J. and D.R.S. determined relative gene expression; W.-S.T. performed confocal microscopy; L.B. performed lipid quantification; D.W., L.E.V., and C.E.B. performed all rabbit infections and provided caseum; A.C. and I.D.V. quantified cell-free DNA (cfDNA); J.P.S. and V.A.D. wrote the manuscript.

REFERENCES

1. Aber VR, Nunn AJ. 1978. Short term chemotherapy of tuberculosis. Factors affecting relapse following short term chemotherapy. Bull Int Union Tuberc 53:276–280.
2. Imperial MZ, Nahid P, Phillips PPJ, Davies GR, Fielding K, Hanna D, Hermann D, Wallis RS, Johnson JL, Lienhardt C, Savic RM. 2018. A patient-level pooled analysis of treatment-shortening regimens for drug-susceptible pulmonary tuberculosis. Nat Med 24:1708–1715. https://doi.org/10.1038/s41591-018-0224-2.
3. Savic RM, Weiner M, MacKenzie WR, Engle M, Whitworth WC, Johnson JL, Nsubuga P, Nahid P, Nguyen NV, Peloquin CA, Dooley KE, Dorman SE, Tuberculosis Trials Consortium of the Centers for Disease Control and Prevention. 2017. Defining the optimal dose of rifapentine for pulmonary tuberculosis: exposure-response relations from two phase II clinical trials. Clin Pharmacol Ther 102:321–331. https://doi.org/10.1002/cpt.634.
4. Kim SH, Shin YM, Yoo JY, Cho JY, Kang H, Lee H, Choe KH, Lee KM, Yang B. 2021. Clinical factors associated with cavitary tuberculosis and its treatment outcomes. J Pers Med 11:1081. https://doi.org/10.3390/jpm11111081.
5. Chen RY, Yu X, Smith B, Liu X, Gao J, Diacon AH, Dawson R, Tameris M, Zhu H, Qu Y, Zhang R, Pan S, Jin X, Goldfeder LC, Cai Y, Arora K, Wang J, Vincent J, Malherbe ST, Thienemann F, Wilkinson RJ, Walzl G, Barry CE. 2021. Radiological and functional evidence of the bronchial spread of tuberculosis: an observational analysis. Lancet Microbe 2:e518–e526. https://doi.org/10.1016/S2666-5247(21)00058-6.
6. Sarathy JP, Dartois V. 2020. Caseum: a niche for Mycobacterium tuberculosis drug-tolerant persisters. Clin Microbiol Rev 33:e00159-19. https://doi.org/10.1128/CMR.00159-19.
7. Kim M, Wainwright HC, Locketz M, Bekker L, Walther GB, Dittrich C, Visser A, Wang W, Hsu F, Wiehart U, Tsenova L, Kaplan G, Russell DG. 2010. Caseation of human tuberculosis granulomas correlates with elevated host lipid metabolism. EMBO Mol Med 2:258–274. https://doi.org/10.1002/emmm.201000079.
8. Hunter RL. 2016. Tuberculosis as a three-act play: a new paradigm for the pathogenesis of pulmonary tuberculosis. Tuberculosis (Edinb) 97:8–17. https://doi.org/10.1016/j.tube.2015.11.010.

9. Hoff DR, Ryan GJ, Driver ER, Ssemakulu CC, De Groote MA, Basaraba RJ, Lenaerts AJ. 2011. Location of intra- and extracellular M. tuberculosis populations in lungs of mice and guinea pigs during disease progression and after drug treatment. PLoS One 6:e17550. https://doi.org/10.1371/journal.pone.0017550.
10. Lenaerts AJ, Hoff D, Aly S, Ehlers S, Andries K, Cantarero L, Orme IM, Basaraba RJ. 2007. Location of persisting mycobacteria in a guinea pig model of tuberculosis revealed by r207910. Antimicrob Agents Chemother 51:3338–3345. https://doi.org/10.1128/AAC.00276-07.
11. Via LE, England K, Weiner DM, Schimel D, Zimmerman MD, Dayao E, Chen RY, Dodd LE, Richardson M, Robbins KK, Cai Y, Hammoud D, Herscovitch P, Dartois V, Flynn JL, Barry CE. 2015. A sterilizing tuberculosis treatment regimen is associated with faster clearance of bacteria in cavitary lesions in marmosets. Antimicrob Agents Chemother 59:4181–4189. https://doi.org/10.1128/AAC.00115-15.
12. Driver ER, Ryan GJ, Hoff DR, Irwin SM, Basaraba RJ, Kramnik I, Lenaerts AJ. 2012. Evaluation of a mouse model of necrotic granuloma formation using C3HeB/FeJ mice for testing of drugs against Mycobacterium tuberculosis. Antimicrob Agents Chemother 56:3181–3195. https://doi.org/10.1128/AAC.00217-12.
13. Kempker RR, Rabin AS, Nikolaishvili K, Kalandadze I, Gogishvili S, Blumberg HM, Vashakidze S. 2012. Additional drug resistance in Mycobacterium tuberculosis isolates from resected cavities among patients with multidrug-resistant or extensively drug-resistant pulmonary tuberculosis. Clin Infect Dis 54:e51–e54. https://doi.org/10.1093/cid/cir904.
14. Kempker RR, Kipiani M, Mirtskhulava V, Tukvadze N, Magee MJ, Blumberg HM. 2015. Acquired drug resistance in Mycobacterium tuberculosis and poor outcomes among patients with multidrug-resistant tuberculosis. Emerg Infect Dis 21:992–1001. https://doi.org/10.3201/eid2106.141873.
15. Dheda K, Lenders L, Magombedze G, Srivastava S, Raj P, Arning E, Ashcraft P, Bottiglieri T, Wainwright H, Pennel T, Linegar A, Moodley L, Pooran A, Pasipanodya JG, Sirgel FA, van Helden PD, Wakeland E, Warren RM, Gumbo T. 2018. Drug-penetration gradients associated with acquired drug resistance in patients with tuberculosis. Am J Respir Crit Care Med 198:1208–1219. https://doi.org/10.1164/rccm.201711-2333OC.
16. Sarathy JP, Via LE, Weiner D, Blanc L, Boshoff H, Eugenin EA, Barry CE, Dartois VA. 2018. Extreme drug tolerance of Mycobacterium tuberculosis in caseum. Antimicrob Agents Chemother 62:e02266-17. https://doi.org/10.1128/AAC.02266-17.
17. Christensen H, Garton NJ, Horobin RW, Minnikin DE, Barer MR. 1999. Lipid domains of mycobacteria studied with fluorescent molecular probes. Mol Microbiol 31:1561–1572. https://doi.org/10.1046/j.1365-2958.1999.01304.x.
18. Deb C, Lee C-M, Dubey VS, Daniel J, Abomoelak B, Sirakova TD, Pawar S, Rogers L, Kolattukudy PE. 2009. A novel in vitro multiple-stress dormancy model for Mycobacterium tuberculosis generates a lipid-loaded, drug-tolerant, dormant pathogen. PLoS One 4:e6077. https://doi.org/10.1371/journal.pone.0006077.
19. Daniel J, Maamar H, Deb C, Sirakova TD, Kolattukudy PE. 2011. Mycobacterium tuberculosis uses host triacylglycerol to accumulate lipid droplets and acquires a dormancy-like phenotype in lipid-loaded macrophages. PLoS Pathog 7:e1002093. https://doi.org/10.1371/journal.ppat.1002093.
20. Low KL, Rao PSS, Shui G, Bendt AK, Pethe K, Dick T, Wenk MR. 2009. Triacylglycerol utilization is required for regrowth of in vitro hypoxic nonreplicating Mycobacterium bovis bacillus Calmette-Guerin. J Bacteriol 191:5037–5043. https://doi.org/10.1128/JB.00530-09.
21. Caire-Brändli I, Papadopoulos A, Malaga W, Marais D, Canaan S, Thilo L, de Chastellier C. 2014. Reversible lipid accumulation and associated division arrest of Mycobacterium avium in lipoprotein-induced foamy macrophages may resemble key events during latency and reactivation of tuberculosis. Infect Immun 82:476–490. https://doi.org/10.1128/IAI.01196-13.
22. Prideaux B, Via LE, Zimmerman MD, Eum S, Sarathy J, O'Brien P, Chen C, Kaya F, Weiner DM, Chen P-Y, Song T, Lee M, Shim TS, Cho JS, Kim W, Cho SN, Olivier KN, Barry CE, Dartois V. 2015. The association between sterilizing activity and drug distribution into tuberculosis lesions. Nat Med 21:1223–1227. https://doi.org/10.1038/nm.3937.
23. Rifat D, Prideaux B, Savic RM, Urbanowski ME, Parsons TL, Luna B, Marzinke MA, Ordonez AA, DeMarco VP, Jain SK, Dartois V, Bishai WR, Dooley KE. 2018. Pharmacokinetics of rifapentine and rifampin in a rabbit model of tuberculosis and correlation with clinical trial data. Sci Transl Med 10:eaai7786. https://doi.org/10.1126/scitranslmed.aai7786.
24. Irwin SM, Prideaux B, Lyon ER, Zimmerman MD, Brooks EJ, Schrupp CA, Chen C, Reichlen MJ, Asay BC, Voskuil MI, Nuermberger EL, Andries K, Lyons MA, Dartois V, Lenaerts AJ. 2016. Bedaquiline and pyrazinamide treatment responses are affected by pulmonary lesion heterogeneity in Mycobacterium tuberculosis infected C3HeB/FeJ mice. ACS Infect Dis 2:251–267. https://doi.org/10.1021/acsinfecdis.5b00127.
25. Strydom N, Gupta SV, Fox WS, Via LE, Bang H, Lee M, Eum S, Shim T, Barry CE, Zimmerman M, Dartois V, Savic RM. 2019. Tuberculosis drugs' distribution and emergence of resistance in patient's lung lesions: a mechanistic model and tool for regimen and dose optimization. PLoS Med 16:e1002773. https://doi.org/10.1371/journal.pmed.1002773.
26. Loebel RO, Shorr E, Richardson HB. 1933. The influence of foodstuffs upon the respiratory metabolism and growth of human tubercle bacilli. J Bacteriol 26:139–166. https://doi.org/10.1128/jb.26.2.139-166.1933.
27. Wayne LG. 2001. In vitro model of hypoxically induced nonreplicating persistence of Mycobacterium tuberculosis. Methods Mol Med 54:247–269.
28. Gold B, Warrier T, Nathan C. 2015. A multi-stress model for high throughput screening against non-replicating Mycobacterium tuberculosis. Methods Mol Biol 1285:293–315. https://doi.org/10.1007/978-1-4939-2450-9_18.
29. Larkins-Ford J, Degefu YN, Van N, Sokolov A, Aldridge BB. 2022. Design principles to assemble drug combinations for effective tuberculosis therapy using interpretable pairwise drug response measurements. Cell Rep Med 3:100737. https://doi.org/10.1016/j.xcrm.2022.100737.
30. Larkins-Ford J, Greenstein T, Van N, Degefu YN, Olson MC, Sokolov A, Aldridge BB. 2021. Systematic measurement of combination-drug landscapes to predict in vivo treatment outcomes for tuberculosis. Cell Syst 12:1046–1063.E7. https://doi.org/10.1016/j.cels.2021.08.004.
31. Peyron P, Vaubourgeix J, Poquet Y, Levillain F, Botanch C, Bardou F, Daffé M, Emile J-F, Marchou B, Cardona P-J, de Chastellier C, Altare F. 2008. Foamy macrophages from tuberculous patients' granulomas constitute a nutrient-rich reservoir for M. tuberculosis persistence. PLoS Pathog 4:e1000204. https://doi.org/10.1371/journal.ppat.1000204.
32. Guerrini V, Prideaux B, Blanc L, Bruiners N, Arrigucci R, Singh S, Ho-Liang HP, Salamon H, Chen P-Y, Lakehal K, Subbian S, O'Brien P, Via LE, Barry CE, Dartois V, Gennaro ML. 2018. Storage lipid studies in tuberculosis reveal that foam cell biogenesis is disease-specific. PLoS Pathog 14:e1007223. https://doi.org/10.1371/journal.ppat.1007223.
33. Leong FJ, Dartois V, Dick T. 2011. A color atlas of comparative pathology of pulmonary tuberculosis. CRC Press, Singapore.
34. Bostrom P, Magnusson B, Svensson PA, Wiklund O, Boren J, Carlsson LMS, Stahlman M, Olofsson SO, Hulten LM. 2006. Hypoxia converts human macrophages into triglyceride-loaded foam cells. Arterioscler Thromb Vasc Biol 26:1871–1876. https://doi.org/10.1161/01.ATV.0000229665.78997.0b.
35. Milosavljevic D, Kontush A, Griglio S, Le Naour G, Thillet J, Chapman MJ. 2003. VLDL-induced triglyceride accumulation in human macrophages is mediated by modulation of LPL lipolytic activity in the absence of change in LPL mass. Biochim Biophys Acta 1631:51–60. https://doi.org/10.1016/S1388-1981(02)00355-4.
36. den Hartigh LJ, Connolly-Rohrbach JE, Fore S, Huser TR, Rutledge JC. 2010. Fatty acids from very low-density lipoprotein lipolysis products induce lipid droplet accumulation in human monocytes. J Immunol 184:3927–3936. https://doi.org/10.4049/jimmunol.0903475.
37. Sarathy JP, Zuccotto F, Hsinpin H, Sandberg L, Via LE, Marriner GA, Masquelin T, Wyatt P, Ray P, Dartois V. 2016. Prediction of drug penetration in tuberculosis lesions. ACS Infect Dis 2:552–563. https://doi.org/10.1021/acsinfecdis.6b00051.
38. Sarathy JP, Liang HPH, Weiner D, Gonzales J, Via LE, Dartois V. 2017. An in vitro caseum binding assay that predicts drug penetration in tuberculosis lesions. J Vis Exp 2017:55559. https://doi.org/10.3791/5555.
39. Blanc L, Sarathy JP, Alvarez Cabrera N, O'Brien P, Dias-Freedman I, Mina M, Sacchettini J, Savic RM, Gengenbacher M, Podell BK, Prideaux B, Ioerger T, Dick T, Dartois V. 2018. Impact of immunopathology on the antituberculous activity of pyrazinamide. J Exp Med 215:1975–1986. https://doi.org/10.1084/jem.20180518.
40. Korem T, Zeevi D, Suez J, Weinberger A, Avnit-Sagi T, Pompan-Lotan M, Matot E, Jona G, Harmelin A, Cohen N, Sirota-Madi A, Thaiss CA, Pevsner-Fischer M, Sorek R, Xavier RJ, Elinav E, Segal E. 2015. Growth dynamics of gut microbiota in health and disease inferred from single metagenomic samples. Science 349:1101–1106. https://doi.org/10.1126/science.aac4812.
41. Koul A, Vranckx L, Dhar N, Göhlmann HW, Özdemir E, Neefs J-M, Schulz M, Lu P, Mørtz E, McKinney JD, Andries K, Bald D. 2014. Delayed bactericidal response of Mycobacterium tuberculosis to bedaquiline involves remodelling of bacterial metabolism. Nat Commun 5:3369. https://doi.org/10.1038/ncomms4369.
42. Dhillon J, Andries K, Phillips PP, Mitchison DA. 2010. Bactericidal activity of the diarylquinoline TMC207 against Mycobacterium tuberculosis outside and within cells. Tuberculosis (Edinb) 90:301–305. https://doi.org/10.1016/j.tube.2010.07.004.

43. Loebel RO, Shorr E, Richardson HB. 1933. The influence of adverse conditions upon the respiratory metabolism and growth of human tubercle bacilli. J Bacteriol 26:167–200. https://doi.org/10.1128/jb.26.2.167-200.1933.
44. Wayne LG, Hayes LG. 1996. An in vitro model for sequential study of shiftdown of Mycobacterium tuberculosis through two stages of nonreplicating persistence. Infect Immun 64:2062–2069. https://doi.org/10.1128/iai.64.6.2062-2069.1996.
45. Conradie F, Diacon AH, Ngubane N, Howell P, Everitt D, Crook AM, Mendel CM, Egizi E, Moreira J, Timm J, McHugh TD, Wills GH, Bateson A, Hunt R, Van Niekerk C, Li M, Olugbosi M, Spigelman M, Nix-TB Trial Team. 2020. Treatment of highly drug-resistant pulmonary tuberculosis. N Engl J Med 382:893–902. https://doi.org/10.1056/NEJMoa1901814.
46. Almeida D, Converse PJ, Li S-Y, Upton AM, Fotouhi N, Nuermberger EL. 2021. Comparative efficacy of the novel diarylquinoline TBAJ-876 and bedaquiline against a resistant Rv0678 mutant in a mouse model of tuberculosis. Antimicrob Agents Chemother 65:e01412-21. https://doi.org/10.1128/AAC.01412-21.
47. Xu J, Converse PJ, Upton AM, Mdluli K, Fotouhi N, Nuermberger EL. 2021. Comparative efficacy of the novel diarylquinoline TBAJ-587 and bedaquiline against a resistant Rv0678 mutant in a mouse model of tuberculosis. Antimicrob Agents Chemother 65:e02418-20. https://doi.org/10.1128/AAC.02418-20.
48. Sarathy J, Blanc L, Alvarez-Cabrera N, O'Brien P, Dias-Freedman I, Mina M, Zimmerman M, Kaya F, Ho Liang H-P, Prideaux B, Dietzold J, Salgame P, Savic RM, Linderman J, Kirschner D, Pienaar E, Dartois V. 2019. Fluoroquinolone efficacy against tuberculosis is driven by penetration into lesions and activity against resident bacterial populations. Antimicrob Agents Chemother 63:e02516-18. https://doi.org/10.1128/AAC.02516-18.
49. Lin PL, Ford CB, Coleman MT, Myers AJ, Gawande R, Ioerger T, Sacchettini J, Fortune SM, Flynn JL. 2014. Sterilization of granulomas is common in active and latent tuberculosis despite within-host variability in bacterial killing. Nat Med 20:75–79. https://doi.org/10.1038/nm.3412.
50. Rastogi S, Agarwal P, Krishnan MY. 2016. Use of an adipocyte model to study the transcriptional adaptation of Mycobacterium tuberculosis to store and degrade host fat. Int J Mycobacteriol 5:92–98. https://doi.org/10.1016/j.ijmyco.2015.10.003.
51. Kondo E, Kanai K. 1972. The lethal effect of long-chain fatty acids on mycobacteria. Jpn J Med Sci Biol 25:1–13. https://doi.org/10.7883/yoken1952.25.1.
52. Kondo E, Kanai K. 1976. Further studies on the lethal effect of long-chain fatty acids on mycobacteria. Jpn J Med Sci Biol 29:25–37. https://doi.org/10.7883/yoken1952.29.25.
53. Lee W, VanderVen BC, Fahey RJ, Russell DG. 2013. Intracellular Mycobacterium tuberculosis exploits host-derived fatty acids to limit metabolic stress. J Biol Chem 288:6788–6800. https://doi.org/10.1074/jbc.M112.445056.
54. Mallick I, Santucci P, Poncin I, Point V, Kremer L, Cavalier J-F, Canaan S. 2021. Intrabacterial lipid inclusions in mycobacteria: unexpected key players in survival and pathogenesis? FEMS Microbiol Rev 45:fuab029. https://doi.org/10.1093/femsre/fuab029.
55. Maurya RK, Bharti S, Krishnan MY. 2019. Triacylglycerols: fuelling the hibernating Mycobacterium tuberculosis. Front Cell Infect Microbiol 8:450. https://doi.org/10.3389/fcimb.2018.00450.
56. Gold B, Nathan C. 2017. Targeting phenotypically tolerant Mycobacterium tuberculosis. Microbiol Spectr 5:TBTB2-0031-2016. https://doi.org/10.1128/microbiolspec.TBTB2-0031-2016.
57. Kreutzfeldt KM, Jansen RS, Hartman TE, Gouzy A, Wang R, Krieger IV, Zimmerman MD, Gengenbacher M, Sarathy JP, Xie M, Dartois V, Sacchettini JC, Rhee KY, Schnappinger D, Ehrt S. 2022. CinA mediates multidrug tolerance in Mycobacterium tuberculosis. Nat Commun 13:2203. https://doi.org/10.1038/s41467-022-29832-1.
58. Dorman SE, Nahid P, Kurbatova EV, Phillips PP, Bryant K, Dooley KE, Engle M, Goldberg SV, Phan HT, Hakim J, Johnson JL, Lourens M, Martinson NA, Muzanyi G, Narunsky K, Nerette S, Nguyen NV, Pham TH, Pierre S, Purfield AE, Samaneka W, Savic RM, Sanne I, Scott NA, Shenje J, Sizemore E, Vernon A, Waja Z, Weiner M, Swindells S, Chaisson RE. 2021. Four-month rifapentine regimens with or without moxifloxacin for tuberculosis. N Engl J Med 384:1705–1718. https://doi.org/10.1056/NEJMoa2033400.
59. Sassetti CM, Boyd DH, Rubin EJ. 2001. Comprehensive identification of conditionally essential genes in mycobacteria. Proc Natl Acad Sci U S A 98:12712–12717. https://doi.org/10.1073/pnas.231275498.
60. Rock JM, Hopkins FF, Chavez A, Diallo M, Chase MR, Gerrick ER, Pritchard JR, Church GM, Rubin EJ, Sassetti CM, Schnappinger D, Fortune SM. 2017. Programmable transcriptional repression in mycobacteria using an orthogonal CRISPR interference platform. Nat Microbiol 2:16274. https://doi.org/10.1038/nmicrobiol.2016.274.
61. Cokol M, Kuru N, Bicak E, Larkins-Ford J, Aldridge BB. 2017. Efficient measurement and factorization of high-order drug interactions in Mycobacterium tuberculosis. Sci Adv 3:e1701881. https://doi.org/10.1126/sciadv.1701881.
62. Subbian S, Tsenova L, Yang G, O'Brien P, Parsons S, Peixoto B, Taylor L, Fallows D, Kaplan G. 2011. Chronic pulmonary cavitary tuberculosis in rabbits: a failed host immune response. Open Biol 1:110016. https://doi.org/10.1098/rsob.110016.
63. Bolger AM, Lohse M, Usadel B. 2014. Trimmomatic: a flexible trimmer for Illumina sequence data. Bioinformatics 30:2114–2120. https://doi.org/10.1093/bioinformatics/btu170.
64. Li H, Durbin R. 2009. Fast and accurate short read alignment with Burrows-Wheeler transform. Bioinformatics 25:1754–1760. https://doi.org/10.1093/bioinformatics/btp324.
65. Burnham P, Dadhania D, Heyang M, Chen F, Westblade LF, Suthanthiran M, Lee JR, De Vlaminck I. 2018. Urinary cell-free DNA is a versatile analyte for monitoring infections of the urinary tract. Nat Commun 9:2412. https://doi.org/10.1038/s41467-018-04745-0.
66. Lakshminarayana SB, Huat TB, Ho PC, Manjunatha UH, Dartois V, Dick T, Rao SPS. 2015. Comprehensive physicochemical, pharmacokinetic and activity profiling of anti-TB agents. J Antimicrob Chemother 70:857–867. https://doi.org/10.1093/jac/dku457.
67. Irwin SM, Driver E, Lyon E, Schrupp C, Ryan G, Gonzalez-Juarrero M, Basaraba RJ, Nuermberger EL, Lenaerts AJ. 2015. Presence of multiple lesion types with vastly different microenvironments in C3HeB/FeJ mice following aerosol infection with Mycobacterium tuberculosis. Dis Model Mech 8:591–602. https://doi.org/10.1242/dmm.019570.
68. Irwin SM, Gruppo V, Brooks E, Gilliland J, Scherman M, Reichlen MJ, Leistikow R, Kramnik I, Nuermberger EL, Voskuil MI, Lenaerts AJ. 2014. Limited activity of clofazimine as a single drug in a mouse model of tuberculosis exhibiting caseous necrotic granulomas. Antimicrob Agents Chemother 58:4026–4034. https://doi.org/10.1128/AAC.02565-14.
69. Lanoix JP, Ioerger T, Ormond A, Kaya F, Sacchettini J, Dartois V, Nuermberger E. 2015. Selective inactivity of pyrazinamide against tuberculosis in C3HeB/FeJ mice is best explained by neutral pH of caseum. Antimicrob Agents Chemother 60:735–743. https://doi.org/10.1128/AAC.01370-15.
70. Botha FJ, Sirgel FA, Parkin DP, van de Wal BW, Donald PR, Mitchison DA. 1996. Early bactericidal activity of ethambutol, pyrazinamide and the fixed combination of isoniazid, rifampicin and pyrazinamide (Rifater) in patients with pulmonary tuberculosis. S Afr Med J 86:155–158.
71. Diacon AH, Dawson R, von Groote-Bidlingmaier F, Symons G, Venter A, Donald PR, van Niekerk C, Everitt D, Hutchings J, Burger DA, Schall R, Mendel CM. 2015. Bactericidal activity of pyrazinamide and clofazimine alone and in combinations with pretomanid and bedaquiline. Am J Respir Crit Care Med 191:943–953. https://doi.org/10.1164/rccm.201410-1801OC.
72. Wallis RS, Dawson R, Friedrich SO, Venter A, Paige D, Zhu T, Silvia A, Gobey J, Ellery C, Zhang Y, Eisenach K, Miller P, Diacon AH. 2014. Mycobactericidal activity of sutezolid (PNU-100480) in sputum (EBA) and blood (WBA) of patients with pulmonary tuberculosis. PLoS One 9:e94462. https://doi.org/10.1371/journal.pone.0094462.
73. Diacon AH, Dawson R, Du Bois J, Narunsky K, Venter A, Donald PR, van Niekerk C, Erondu N, Ginsberg AM, Becker P, Spigelman MK. 2012. Phase II dose-ranging trial of the early bactericidal activity of PA-824. Antimicrob Agents Chemother 56:3027–3031. https://doi.org/10.1128/AAC.06125-11.
74. Diacon AH, Dawson R, Von Groote-Bidlingmaier F, Symons G, Venter A, Donald PR, Conradie A, Erondu N, Ginsberg AM, Egizi E, Winter H, Becker P, Mendel CM. 2013. Randomized dose-ranging study of the 14-day early bactericidal activity of bedaquiline (TMC207) in patients with sputum microscopy smear-positive pulmonary tuberculosis. Antimicrob Agents Chemother 57:2199–2203. https://doi.org/10.1128/AAC.02243-12.
75. Diacon AH, De Jager VR, Dawson R, Narunsky K, Vanker N, Burger DA, Everitt D, Pappas F, Nedelman J, Mendel CM. 2020. Fourteen-day bactericidal activity, safety, and pharmacokinetics of linezolid in adults with drug-sensitive pulmonary tuberculosis. Antimicrob Agents Chemother 64:e02012-19. https://doi.org/10.1128/AAC.02012-19.
76. Johnson JL, Hadad DJ, Boom WH, Daley CL, Peloquin CA, Eisenach KD, Jankus DD, Debanne SM, Charlebois ED, Maciel E, Palaci M. 2006. Early and extended early bactericidal activity of levofloxacin, gatifloxacin and moxifloxacin in pulmonary tuberculosis. Int J Tuber Lung Dis 10:605–612.
77. Sirgel FA, Botha FJH, Parkin DP, Van De Wal BW, Donald PR, Clark PK, Mitchison DA. 1993. The early bactericidal activity of rifabutin in patients with pulmonary tuberculosis measured by sputum viable counts: a new

method of drug assessment. J Antimicrob Chemother 32:867–875. https://doi.org/10.1093/jac/32.6.867.

78. Sirgel FA, Fourie PB, Donald PR, Padayatchi N, Rustomjee R, Levin J, Roscigno G, Norman J, McIlleron H, Mitchison DA. 2005. The early bactericidal activities of rifampin and rifapentine in pulmonary tuberculosis. Am J Respir Crit Care Med 172:128–135. https://doi.org/10.1164/rccm.200411-1557OC.
79. Heinrich N, Dawson R, Du Bois J, Narunsky K, Horwith G, Phipps AJ, Nacy CA, Aarnoutse RE, Boeree MJ, Gillespie SH, Venter A, Henne S, Rachow A, Phillips PPJ, Hoelscher M, Diacon AH, Mekota AM, Heinrich N, Rachow A, Saathoff E, Hoelscher M, Gillespie S, Colbers A, van Balen GP, Aarnoutse R, Boeree M, Bateson A, McHugh T, Singh K, Hunt R, Zumla A, Nunn A, Phillips P, Rehal S, Dawson R, Narunsky K, Diacon A, Du Bois J, Venter A, Friedrich S, Sanne I, Mellet K, Churchyard G, Charalambous S, Mwaba P, Elias N, Mangu C, Rojas-Ponce G, Mtafya B, Maboko L, Pan African Consortium for the Evaluation of Antituberculosis Antibiotics (PanACEA). 2015. Early phase evaluation of SQ109 alone and in combination with rifampicin in pulmonary TB patients. J Antimicrob Chemother 70:1558–1566. https://doi.org/10.1093/jac/dku553.
80. Shirude PS, Shandil RK, Manjunatha MR, Sadler C, Panda M, Panduga V, Reddy J, Saralaya R, Nanduri R, Ambady A, Ravishankar S, Sambandamurthy VK, Humnabadkar V, Jena LK, Suresh RS, Srivastava A, Prabhakar KR, Whiteaker J, McLaughlin RE, Sharma S, Cooper CB, Mdluli K, Butler S, Iyer PS, Narayanan S, Chatterji M. 2014. Lead optimization of 1,4-azaindoles as antimycobacterial agents. J Med Chem 57:5728–5737.